ACS Catalysis

Research Article

pubs.acs.org/acscatalysis

Impact of Process Conditions on the Sintering Behavior of an Alumina-Supported Cobalt Fischer–Tropsch Catalyst Studied with an in Situ Magnetometer

M. Claeys,*[,†] M. E. Dry,[†] E. van Steen,[†] P. J. van Berge,[‡] S. Booyens,[‡] R. Crous,[‡] P. van Helden,[‡] J. Labuschagne,[‡] D. J. Moodley,[‡] and A. M. Saib[‡]

[†]Centre for Catalysis Research, Department of Chemical Engineering, University of Cape Town, Rondebosch 7701, South Africa

[‡]Sasol Technology (Pty) Ltd., P.O. Box 1, Sasolburg 1947, South Africa

ABSTRACT: Sintering of supported cobalt nanoparticles is one of the main deactivation mechanisms in the Fischer–Tropsch synthesis. In this study, crystallite growth was studied with an alumina-supported catalyst in real time and as a function of process conditions using a novel in situ magnetometer. It could be shown that sintering with this catalyst occurred via a combination of high CO and high water partial pressures. It is proposed that particle growth proceeds via cobalt subcarbonyl migration over the hydroxylated support surface.

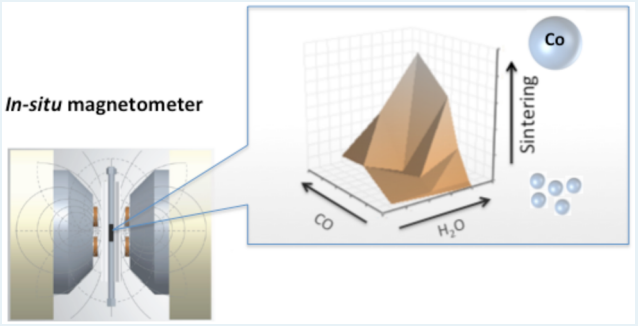

KEYWORDS: *Fischer–Tropsch synthesis, cobalt catalysts, sintering, oxidation, in situ magnetic measurements, reaction conditions, water, carbon monoxide, temperature*

1. INTRODUCTION

Supported cobalt Fischer–Tropsch (FT) catalysts are commercially used by Sasol and Shell in GTL plants in Qatar and Malaysia. Cobalt is a relatively expensive metal, and the catalyst stability is of utmost importance for the economics of these processes.[1] As with any other catalytic conversion, the Fischer–Tropsch synthesis is affected by catalyst deactivation. The main deactivation mechanisms proposed for cobalt FTS are[1−3] (1) oxidation, (2) metal–support solid-state reactions, (3) carbon deposition and carburization, (4) sintering, (5) poisoning, (6) surface reconstruction, and (7) mechanical attrition. Among these, carbon deposition and sintering have been identified as the major contributors to the overall deactivation of the catalyst.[1] Sintering has been reported to account for up to 30–40% of the activity loss of an alumina-supported cobalt catalyst tested in a slurry bubble column reactor at commercially relevant FTS conditions.[4,5]

The sintering process is thermodynamically driven resulting in growth of crystallites at the expense of smaller crystallites due to the difference in surface energy.[1,3,6] In a cobalt FT catalyst, nanosized cobalt particles are present on a suitable support material (e.g., Al_2O_3, TiO_2, SiO_2). Sintering can generally occur via two mechanisms, namely, via migration of atoms (Ostwald ripening) or via particle migration over the support followed by coalescence. The rate of sintering is mainly affected by temperature, metal and support type, and the reaction atmosphere; in particular, water is known to cause/enhance sintering.[1,3,6,7] The so-called Tamman and Hüttig temperatures, which are related to the melting temperature of a material ($T_{Hüttig} = 0.3T_{melting}$, $T_{Tamman} = 0.5T_{melting}$), may give an indication at which temperature sintering is to be expected.[6] Generally, with increasing temperature, the mobility of atoms increases. When the Hüttig temperature is reached, atoms at defects will become mobile, while at the Tamman temperature, atoms from the bulk will exhibit mobility. For cobalt, these temperatures are 253 and 604 °C, respectively. Moreover, smaller particles have a higher chemical potential due to the surface energy contribution providing a larger driving force for diffusion,[8] and thus, sintering may be expected even at the fairly mild temperatures of the low-temperature FT reaction. Metal–support interaction may counteract these effects and provide some stability against sintering. In this regard, for example, alumina supports are considered to provide more stability than silica in cobalt FT catalysts, due to improved metal–support interaction.[1] However, the reaction atmosphere can also impact on the catalyst stability and even cause sintering (e.g., via the formation of relatively volatile compounds).[6] Sintering is therefore a complex process affected by a variety of parameters.

Only a limited number of studies are available highlighting the importance of sintering in cobalt-based Fischer–Tropsch synthesis. These studies largely rely on chemisorption, conventional TEM, and XRD, as well as synchrotron radiation based spectroscopic techniques for crystallite size determination and mostly focus on external catalyst characterization

Received: November 14, 2014
Published: December 17, 2014

DOI: 10.1021/cs501810y
ACS Catal. 2015, 5, 841–852

(i.e., before and/or after exposure to the corresponding FT test conditions).

Bian et al. studied two impregnated Co/SiO_2 catalysts with different initial average crystallite sizes (10 and 29 nm, determined by means of H_2-chemisorption) in the FT synthesis at 10 bar and at 200 and 240 °C ($H_2/CO = 2$).[9] Although almost no sintering was observed at the lower temperature, significant crystallite growth of the smaller crystallites (from 10 to 16 nm) was found in the spent catalysts after exposure to 240 °C. Only a marginal change in crystallite size was observed at these conditions for the larger crystallites. An increase of the conversion level at 240 °C from 40 to 90% caused a further crystallite growth by 1 nm, which indicates that not only temperature and crystallite size but also the reaction conditions (in this case, an increase of the water partial pressure or the water to syngas ratio, respectively) have an impact on sintering.

Bezemer et al. conducted an in situ Mössbauer model study using a carbon nanofiber-supported cobalt catalyst with a cobalt crystallite size of 5 nm, which was exposed to various H_2O/H_2 mixtures at 20 bar and 200−220 °C simulating high conversion FT conditions.[10] Remarkably, no oxidation was observed in the presence of hydrogen, even at a H_2O/H_2 ratio of 30. A decrease of the amount of superparamagnetic material from 42 to 23% in a test conducted at a H_2O/H_2 ratio of 1 at 200 °C and relatively high absolute water partial pressures (9.6 bar) indicated pronounced sintering, which was also confirmed via TEM/HAADF analysis of the spent catalyst which had an average crystallite size of 21 nm. Due to this loss of metal surface area the spent catalyst also showed a much lower FT activity (73% lower) compared to the fresh catalyst. The authors suggested that the presence of cobalt hydroxyl groups might have enabled migration over the wetted support and therefore sintering via particle coalescence; however, they conceded that the data does not allow one to exclude Ostwald ripening as a mechanism of sintering.

Kiss et al. observed a crystallite size increase from 5 to 11 nm by means of TEM evaluation of a Co/SiO_2 catalyst which was exposed to FT conditions of 220 °C, $H_2/CO = 2.1$, 35 bar, and high syngas conversion (>90%), and therefore high water partial pressures in a fixed bed reactor.[11] Solid-state reactions with formation of cobalt−silica mixed oxide were noticed during these studies. These authors later proposed initial (reversible) cobalt surface oxidation which would lead to "wetting" of the support surface with cobalt oxide islands and subsequent formation of larger metallic cobalt particles.[12]

Cobalt sintering, coinciding with catalyst deactivation, was also observed on an alumina-supported catalyst by Khodakov et al. during the first hours of testing at realistic FT conditions (220 °C, 20 bar, $H_2/CO = 2$) using in situ synchrotron XRD measurements.[13,14] Interestingly they claimed that sintering was limited to the fcc-cobalt allotrope and not observed for the cobalt hcp phase. They further report enhanced sintering (4.3 to 8.5 nm) with a decrease of the H_2/CO inlet ratio from 4 to 2 to 1 and particle growth (from 6.1 to 9.8 nm) with an increase of reaction temperature by 20 °C.[15] Enhanced sintering at a low H_2/CO ratio 1 had earlier also been observed during the FTS with a Co/SiO_2 catalyst by Zhou et al. (2006).[16] In analogy to a sintering model (which assumes particle migration mediated by oxidized adatoms) developed for the high-temperature nickel steam reforming catalysts by Sehested et al.,[17−19] Khodakov et al. proposed a similar mechanism for cobalt-based FTS assuming temporary cobalt surface oxidation leading to enhanced diffusivity and particle migration, ultimately resulting in crystallite growth.[15,20,21] Bulk oxidation of cobalt nanocrystallites had earlier been concluded to only play a negligible role at relevant FT conditions as only very small crystallites (i.e., < 5 nm) are affected.[1,5,22,23]

The group of Davis has used synchrotron based techniques, extended X-ray absorption fine structure (EXAFS) analyses, and X-ray absorption near-edge spectroscopy (XANES), on spent alumina-supported cobalt catalysts, some promoted with platinum, ruthenium, and rhenium, which had been tested in a slurry reactor at 220 °C and 18 bar ($H_2/CO = 2$) and reported an increase of the Co−Co coordination as a function of time on stream and compared to a freshly reduced sample possibly indicating sintering.[24−28] It was noticed though that the increase of the Co−Co coordination may also be caused by further reduction of unreduced CoO,[28] which was also observed by others.[1,2,29−32]

On the basis of postrun XRD and H_2-chemisorption analyses, Tavasoli et al. also identified sintering as the main long-term deactivation mechanisms for a ruthenium-promoted Co/Al_2O_3 catalyst tested in a fixed bed reactor (220 °C, 20 bar, $H_2/CO = 2$).[33,34] The change in cobalt crystallite size as a function of time was modeled using a power law expression.[34] Slightly increased crystallite sizes (6% growth) were observed along the catalyst bed, suggesting more pronounced sintering at conditions of high water to syngas ratios or high water partial pressures, respectively. The authors also noticed increased formation of metal oxides (cobalt aluminates) toward the bottom of the catalyst bed.

Combined in situ XRD and XANES studies were conducted by Rønning et al. using a Re-promoted $Co/\gamma\text{-}Al_2O_3$ catalyst[30] and a carbon-supported cobalt model catalyst.[31] When testing the former catalyst, no sintering was observed at 210 °C and 18 bar ($H_2/CO = 2.1$), although some crystallite growth and further catalyst reduction were noticed at methanation conditions (400 °C, 10 bar, $H_2/CO = 2.1$). With the carbon-supported model catalyst, however, sintering from 18 to 22 nm was observed to occur in the first 10 h of testing (at 215 °C, 18 bar, $H_2/CO = 2.1$), which also coincided with further catalyst reduction.[31] This indicates the importance of the role of the support and metal−support interaction on crystallite sintering. In a recent study, Tsakoumis et al. reported significant sintering and further reduction of the Re-promoted $Co/\gamma\text{-}Al_2O_3$ catalyst, which was exposed to industrial FT conditions (210−240 °C, $H_2/CO = 2$) for several weeks in a semicommercial slurry phase reactor.[32] A comparison of the TEM analyses of the freshly reduced and the spent catalyst indicate growth of the average cobalt crystallite particle size from 11.5 to 16.9 nm, which approximately corresponds to a 30% loss of metal surface area. Crystallite migration was concluded as the most likely sintering mechanism as judged from particle size distributions together with the spread of Co nanoparticles over the support. It should be noted that drawing conclusions from particle size distributions when there are small shifts in crystallite sizes can be problematic. Datye et al. stated that particle-size distributions are typically represented by a log-normal distribution, and thus, no inference can be made about sintering mechanism from these distributions.[35]

Overett et al. conducted a detailed TEM/HAADF analysis of fresh and spent samples of a platinum promoted Co/Al_2O_3 catalyst, which was tested at commercially relevant FTS conditions (230 °C, 20 bar, $H_2/CO = 2$, (H_2 + CO) conversion between 50 and 70%) in a 100 bbl/day slurry bubble column reactor.[4] The reduced catalyst prior to testing

DOI: 10.1021/cs501810y
ACS Catal. 2015, 5, 841−852

showed a range of particles sized between 3 and 15 nm with a maximum abundance of around 6 nm, which corresponded to a surface-area-weighted average cobalt crystallite size of 9.5 nm. The average diameter increased to about 15 nm in the spent catalyst. It could be shown that this crystallite growth mostly occurred during the first few days of FTS. Assuming a direct correlation between cobalt metal surface area and cobalt catalyst activity, it was estimated that sintering can contribute about 30 to 40% of the observed loss in activity.[4,5] This loss in activity can represent a significant challenge in the commercial FT process and once a catalyst has sintered, the corresponding activity loss can only be recovered via catalyst regeneration.[1,5,36,37]

The above studies demonstrate that sintering can indeed play an important role in the cobalt-catalyzed FT synthesis. However, detailed information on the effect of reaction conditions on crystallite growth is very limited. Generally, the presence of water has been associated with crystallite growth in FTS, and particle migration mechanisms have been put forward by several groups. Moreover, some studies suggest low H_2/CO ratio and increased temperatures to enhance sintering. It may further be noted that most of the investigations reported above rely on external characterization of spent catalyst, which may undergo changes during air exposure or during washing steps for wax removal. In this study, we present a detailed and systematic study on the sintering process as a function of reaction parameters such as temperature, and partial pressures of H_2O and CO. The study was conducted using the in situ magnetometer at the University of Cape Town, which allows the investigation of phase and crystallite size changes at fully relevant industrial FT conditions in real time.[23,38,39] A platinum-promoted Co/Al_2O_3 catalyst was used in the study, which is complimented by TEM-HAADF characterization of some of the spent catalyst samples.

2. METHODS AND MODELS

2.1. Catalyst. The cobalt catalyst (20 wt % Co/Al_2O_3, promoted with 0.05 wt % platinum) used in this study was prepared via slurry impregnation of a γ-alumina support (Puralox 2/150, Sasol Germany) with an aqueous cobalt nitrate solution, also containing platinum. Two consecutive impregnation steps were performed in order to achieve the targeted cobalt loading. After each step, the catalyst was dried and calcined in air at 250 °C.[40] The cobalt crystallites in this catalyst, in its reduced form, are sized between 3 and 15 nm with maximum abundance of around 6 nm, and these crystallites are mostly arranged in clusters of approximately 50−100 nm in diameter.[4,5]

2.2. In Situ Magnetic Measurements. The experiments to study sintering and reduction/oxidation as a function of process conditions were conducted using the in situ setup for magnetic measurements at the University of Cape Town, South Africa.[23,38,39] This setup is based on the Weiss extraction method, and it uses a field-controlled electromagnet, which provides field strengths of up to 20 kOe (2.0 T). Catalysts (in this study, 0.5 g diluted with 1 g of γ-Al_2O_3) are placed in a fixed bed reactor, which can be operated at high temperatures (600 °C and higher) and high pressures (50 bar and higher).

The saturation magnetization (M_{sat}) is directly proportional to the amount of metallic cobalt present, which can be quantified after calibration of the system with known amounts of cobalt. From this the degree of reduction can be determined as being the percentage of metallic cobalt of the amount of cobalt loaded in the fresh catalyst. In this study it is assumed that the saturation magnetization is independent of crystallite size;[41] only very small crystallites (i.e., smaller than 2 nm) display a somewhat larger magnetic moment.[42] It should be noted that the saturation magnetization can also be affected by species adsorbing on the surface of cobalt crystallites. A theoretical estimate of this adsorbed species effect is given below.

In order to obtain information regarding crystallite growth, the remnant magnetization (M_{rem}), that is, the magnetization at 0 kOe, was measured after each measurement of saturation magnetization. The mass fraction, γ, of cobalt in magnetic domains larger than the critical diameter (D_C) is then calculated from the remnant and the saturation magnetization as being $\gamma = 2*M_{rem}/M_{sat}*100\%$. At room temperature D_C for cobalt has been reported to be approximately 15−20 nm at room temperature.[43−45] Bean and Livingstone gave theoretical values of 8 nm for hcp cobalt and 28 nm for fcc cobalt at room temperature.[46] This critical diameter increases with increasing temperature and γ therefore decreases with temperature ($D_C \propto T^{1/3}$). The exact value for D_C is not known and not of importance for this study as γ—or rather, changes (increases) in γ—were used as a semiquantitative indicator for crystallite size growth/sintering. Importantly, these changes, which were confirmed by TEM analyses of spent catalysts, could be measured in real time and at reaction conditions as a measurement of saturation magnetization followed by remnant magnetization, all of which takes about 2 min.

Process conditions were simulated via feeding H_2 and CO at high space velocities and therefore negligible water formation (syngas conversion <15%). Different water partial pressures were then obtained via addition of water to the feed using an HPLC pump and a vaporizer. Inlet and outlet lines of the reactor were heated in order to avoid condensation. Water partial pressures of up to 8 bar could be realized. The reaction conditions were varied over a wide range with emphasis on studies on the effect of temperature (210−250 °C) and a variation of CO/syngas and water partial pressures over a wide range. In addition experiments with hydrogen−water mixtures (i.e., without CO) were conducted. The exact reaction conditions are given in the corresponding results sections below. The exposure to FT conditions was between 2 and 120 h. In order to avoid initial exotherms, the runs were started up at reaction pressure in a hydrogen and water vapor atmosphere, and CO was blended in stepwise over the duration of 1 h. During all steps, magnetic readings were taken. Prior to the FT testing, the catalyst was reduced in hydrogen (80 mL/min (STP)) at 1 bar using a heating rate of 1 °C/min. The reduction was stopped when a degree of reduction of 65 to 70% was reached (typically at a temperature of 380−400 °C).

2.3. TEM Characterization. Scanning Transmission Electron Microscopy (STEM) measurements were performed on selected spent catalyst samples using a field emission FEI Tecnai F20 microscope, operated at 200 kV, which was equipped with a high-angle annular dark-field (HAADF) detector for Z-contrast imaging and coupled with an energy dispersive X-ray spectrometer (EDX) for elemental analysis. Prior to measurements, the catalyst materials were sonicated in ethanol and supported onto lacey carbon coated copper grids (SPI Supplies, 200 mesh). Before removal of the catalyst samples after experimental runs in the in situ setup for magnetic measurements, the samples were passivated by flowing CO_2 over the sample at room temperature for 1 h.

DOI: 10.1021/cs501810y
ACS Catal. 2015, 5, 841−852

2.4. Computational Methods. All quantum chemical calculations in this study were performed using the Vienna Ab initio Simulation Package (VASP).[47,48] The spin-polarized generalized gradient approximation (GGA) with the Perdew and Wang exchange−correlation functional (PW91) with ultrasoft pseudopotentials was used.[49] The electron smearing at the Fermi level was performed using by the Methfessel and Paxton approach with σ = 0.2 eV.[50]

Three surfaces were considered: The two prominent FCC terrace surfaces Co(111) and Co(100) and a step surface to study the effect of adsorption on defects. A five-layer slab was used for the Co(111) surface and a four layer slab was used for the Co(100) surface. The surfaces were represented by using p(2 × 2) surface unit cells. This is equivalent to a coverage of 0.25 ML. These models have a 10 Å vacuum layer between the repeating surfaces. The bottom two layers of both slabs were constrained while all the other atoms in the configurations were allowed to relax upon optimization. The k-point sampling was generated by following the Monkhorst−Pack procedure with a 9 × 9 × 1 mesh for the Co(111) surface and a 5 × 5 × 1 mesh for the Co(100) surface.[51] The plane wave basis set cutoff energy was set at 400 eV. The stepped Co(211) surface was represented by using a p(1 × 2) surface unit cell. A four-layer slab was used for the Co(211), with the bottom layer of atoms constrained. The k-point sampling was performed with a 6 × 7 × 1 mesh.

The equilibrium lattice constant and bulk modulus of the FCC Co bulk cell was obtained by fitting various bulk Co cells to the Birch−Murnaghan equation of state.[52,53] Lattice parameter of 3.538 Å was obtained together with a bulk modulus of 202 GPa and a magnetic moment of 1.67 μB per Co atom. These values are in agreement with the experimental values of bulk FCC Co (3.550 Å,[54] 191 GPa,[55] and 1.70 μB,[56] respectively). The corrected average surface energies of 2.79 J·m^{-2} and 3.20 J·m^{-2} were obtained for the Co(111) and Co(100) slabs,[57] respectively, which are in the same range as the experimental estimate of 2.52 J·m^{-2}.[58] The adsorption of the considered intermediates has been done on a single side of the Co surface slabs with dipole corrections to avoid artificial dipoles. The surface atom magnetic moment (M_{surf}) for a clean surface was obtained by

$$M_{surf} = \frac{M_{slab} - N_{slab}M_{bulk}}{N_{surf}} + M_{bulk}$$

where M_{slab} is the total magnetization of the slab, M_{bulk} is the bulk magnetic moment, N_{slab} is the number of Co atoms in the surface unit cell and N_{surf} is the total number of surface Co atoms. An estimate of the change in surface magnetic moment (ΔM) due to adsorption can be calculated by

$$\Delta M = \frac{M_{ads} - M_{slab}}{N_{surf}}$$

where M_{ads} is the total magnetization of the surface with the adsorbed species and N_{surf} is the number of Co atoms on surface where the adsorption takes place. This gives the change in magnetization per surface Co atom due to adsorption at about 0.25 ML coverage. The percentage change is reported relative to the surface magnetic moment.

3. RESULTS

3.1. Computational Results. The resulting calculated changes in magnetization due to adsorption of selected adsorbed species can be seen in Figure 1 and Table 1.

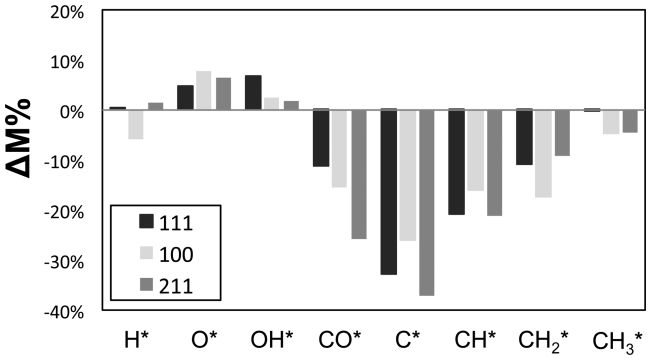

Figure 1. Comparison of the percentage changes in surface magnetization due to adsorption of various FTS intermediates.

Longer hydrocarbon chains were not considered at this stage, but the effect of these chains on the magnetization should be in a similar range to that of the CH_x species. From Table 1, it is clear that upon the creation of a surface, the magnetization of the resulting surface atoms increase for all three surfaces. Figure 1 shows that upon H adsorption, the three surfaces behave somewhat differently, ranging from no effect on Co(111) to a small demagnetization of the Co(100) surface atoms. On all three surfaces, the O and OH intermediates increase the magnetization of the surface atoms. In all cases, the CO and CH_x intermediates will demagnetize the various surfaces. The biggest effect is due to atomic carbon, which can severely affect the magnetization. As the C atom is systematically hydrogenated, the demagnetization is lifted up to the CH_3 intermediate, which has no effect on the Co(111) surface.

It is therefore clear that if there is a large amount of O and OH present on Co surfaces, it could result in an increase in the observed saturation magnetization. The adsorption of CO and its conversion to hydrocarbon intermediates will subsequently lead to a decrease in the saturation magnetization. It is however important to note that these calculations were done at 0.25 ML and that changes in coverage, coadsorption structures and the combined presence of these species, and longer hydrocarbon intermediates could change this picture significantly. Furthermore, considering typical Co active metal surface areas of between 10 m^2·g^{-1} and 15 m^2·g^{-1}, along with the surface areas of the considered sites, only between 1.6% and 2.9% of all the Co atoms will be located at the surface. Together with the relative changes in magnetization reported here, we estimate that the expected magnitude of the change in the mass based saturation magnetization due to the effect of specific adsorbed species should be in the order of about 1% at 0.25 ML coverage. Higher coverages of these species could have a more pronounced effect.[59]

3.2. Experimental Results. *3.2.1. Variation of Temperature.* Three experiments were conducted to study the effect of reaction temperature on sintering. The corresponding reaction conditions are listed in Table 2.

Figure 2 (left) shows the saturation magnetization for the three experiments. The initial exposure to the hydrogen/water mixture (−90 to −60 min) leads to a small increase of the magnetization, which is due to electronic effects of O and OH

DOI: 10.1021/cs501810y
ACS Catal. 2015, 5, 841−852

Table 1. Calculated Changes in the Magnetic Moments of the Surface Atoms of FCC-Co Surfaces Due to the Adsorption of Various FTS Intermediates at an Equivalent of 0.25 ML Coverage

system	species	M_{surf} (μ_B/Co atom)[a]	ΔM (μ_B/Co atom)[b]	ΔM% (%)
bulk		1.67		
111	clean surface	1.73		
	H*		0.00	0.0
	O*		0.08	4.6
	OH*		0.12	6.9
	CO* (br)		−0.21	−12.1
	CO* (fcc)		−0.20	−11.6
	CO* (hcp)		−0.23	−13.3
	CO* (top)		−0.19	−11.0
	C*		−0.57	−32.9
	CH*		−0.36	−20.8
	CH_2*		−0.19	−11.0
	CH_3*		−0.00	0.0
100	clean surface	1.77		
	H*		−0.11	−6.2
	O*		0.14	7.9
	OH*		0.04	2.3
	H_2O*		−0.02	−1.1
	CO* (hollow)		−0.27	−15.3
	CO* (br)		−0.28	−15.8
	CO* (top)		−0.21	−11.9
	C*		−0.46	−26.0
	CH*		−0.28	−15.8
	CH_2*		−0.31	−17.5
	CH_3*		−0.09	−5.1
211	clean surface	1.79		
	H*		0.02	1.1
	O*		0.09	5.0
	OH*		0.02	1.1
	CO*		−0.35	−19.6
	C*		−0.50	−27.9
	CH*		−0.28	−15.6
	CH_2*		−0.12	−6.7
	CH_3*		−0.06	−3.7

[a]The calculated magnetic moment of each Co surface atom. [b]Change in the magnetic moment per Co atom affected by the adsorption.

Table 2. Reaction Conditions (Average Reactor Partial Pressures and Temperature) for 3 h Exposure Runs Performed with Co/Pt/Al_2O_3 Catalyst − Variation of Reaction Temperature[a]

run number	p_{H_2} (bar)	p_{CO} (bar)	p_{H_2O} (bar)	temperature (°C)
variation of temperature				
1	9.3	5.8	5.6	210
2	9.3	5.8	5.6	230
3	9.3	5.8	5.6	250

[a]Note that water partial pressures were realized via water co-feeding; syngas conversion was kept below 15%.

groups present on the surface of cobalt crystallites. This is followed by a slight decrease upon the slow introduction of CO (−60 to 0 min) as expected upon adsorption of an electrophilic species. These two observations correspond very well to the calculated changes in saturation magnetization shown above. At time 0 min, steady-state feeding conditions are reached, and the changes in magnetization are not very pronounced. This was also observed in all other runs reported below (and therefore not shown explicitly), unless otherwise noted.

In Figure 2 (right), the weight percentage of cobalt displaying remnant magnetization at reaction temperature is shown (note that the temperature dependency of this value due to the temperature dependency of D_C can be neglected for the range in which the temperature was varied). The exposure to the hydrogen and water atmosphere did not lead to any changes of this value (of around 12 to 15 wt %), indicating absence of particle growth yielding particles larger than the critical diameter (i.e., absence of significant or any sintering due to water). The effect of water will be analyzed in more detail below. Interestingly, the introduction of CO leads to a very significant increase of γ indicative of strong sintering and highlighting that CO is playing a role in this. This increase continues, although less pronounced, at steady-state syngas and water feeding conditions. It can further be noted that at the highest temperature, the change of γ is the largest. The following changes of the percentage of cobalt displaying remnant magnetization ($\Delta\gamma$) or large crystallites, respectively, were obtained during the exposure to FT conditions (including the blending in of CO) at the three different temperatures: 3.0% (210 °C), 5.5% (230 °C), and 10.4% (250 °C).

The effect of temperature on sintering was also studied in the absence of CO, that is, in a hydrogen−water mixture (p_{H_2} = 7.7 bar and p_{H_2O} = 8.0 bar). The exposure time at each temperature was 1 h, followed by 15 min exposure to hydrogen only. Considering the large rise in temperature up to 400 °C, a relatively small increase of γ was observed (see Figure 3). This increase during exposure only occurred from temperatures of 350 °C onward, indicating that sintering in the absence of CO occurs at much higher temperatures than in the presence of it. It should be noted though that γ is temperature-dependent and expected to decrease with an increase in temperature (in the absence of sintering). Measurements at 230 °C after the 350 and 400 °C readings show the actual degree of sintering which is due to temperature.

3.2.2. Variation of CO/Syngas and Water Partial Pressure. Various experiments with variation of reaction conditions have been conducted at a temperature of 230 °C with the aim to deconvolute the effects of water and CO or syngas, respectively. In these experiments, the ratio of H_2/CO was kept at a relatively low value of 1.1, a condition known to promote sintering.[16] The conditions that were realized are listed in Table 3. They have been clustered according to the parameter, which was kept constant at different levels ("low", "medium", "high"), that is, the CO/syngas partial pressure or the water partial pressure, as well as the parameter, which was varied (see subheadings in Table 3). The exposure time in these experiments was 48 to 145 h.

Figure 4 shows the effect of variation of the water partial pressure at the different levels of CO or syngas partial pressure respectively on sintering as expressed in terms of weight percentage of cobalt displaying remnant magnetization, γ. At the low CO partial pressure condition, virtually no change of γ was observed, which indicates the absence of sintering (see Figure 4, top). With an increase in the CO partial pressure or syngas pressure, respectively, (Figure 4, middle and bottom)

DOI: 10.1021/cs501810y
ACS Catal. 2015, 5, 841−852

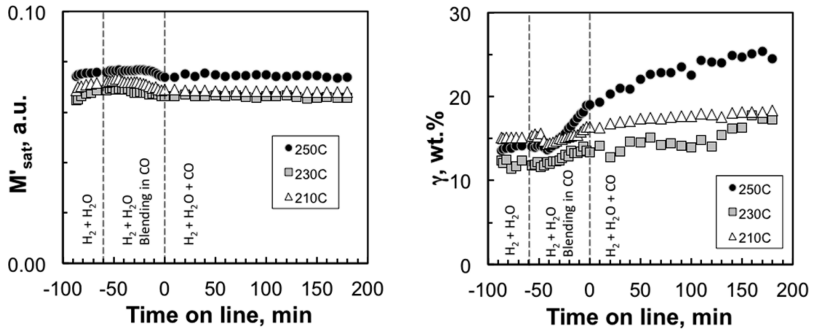

Figure 2. Saturation magnetization, per gram of cobalt in catalyst, (left) and weight percentage of cobalt displaying remnant magnetization, γ, (right) during startup and FTS at three different temperatures.

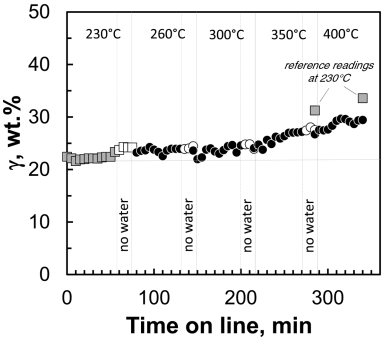

Figure 3. Weight percentage of cobalt displaying remnant magnetization, γ, during exposure to a hydrogen−water mixture at different temperatures (note that after exposure to 350 and 400 °C, readings at 230 °C were also taken to allow for comparison with γ at the starting condition).

clearly an increase of sintering is found which is more severe with an increase of the water partial pressure. In these experiments, sintering mostly seems to come to a conclusion after around 24 to 48 h (see Figure 4 right), as γ only changes slightly thereafter.

Analogously, at fixed water partial pressures, an increase of sintering is observed with an increase of the CO partial pressure or the syngas partial pressure, respectively (see Figure 5). These effects are most pronounced at the highest water partial pressure and the highest syngas partial pressure tested where γ reaches values of over 40 wt %; this means that at reaction temperature, more than 40 wt % now consists of particles with sizes larger than the critical domain size, compared to 10 to 15 wt % in the catalyst after reduction.

The results with regard to the sintering observed in the above series are summarized in Figure 6. Here the differences of γ (as an indication of sintering) after 3 and 48 h are shown relative to initial values at 0 h as a function of the partial pressures of water and CO. It can clearly be seen that sintering is strongly enhanced at high CO and high water partial pressures. In particular, a combination of CO and water seems to be detrimental for the catalyst stability. At low CO partial pressures, almost no sintering occurs, even at high water partial pressures. It should be noted that this change of the weight percentage of cobalt displaying remnant magnetization is not due to potential changes of the ratio of hcp to fcc cobalt, because this remains unaffected as shown via analyses of fresh and spent catalyst.

Selected spent catalyst samples were analyzed by means of TEM analyses (using STEM-HAADF and EDX techniques).

Table 3. Reaction Conditions (Average Reactor Partial Pressures, T = 230°C) for Runs Performed with Co/Pt/Al_2O_3 Catalyst − Variation of CO/Syngas and Water Partial Pressure[a]

run number	p_{H_2} (bar)	p_{CO} (bar)	p_{H_2O} (bar)	p_{H_2O}/p_{H_2}
(a) variation of water partial pressure at fixed "low" CO partial pressure of 0.4 bar				
4	0.5	0.4	1.0	2.10
5	0.5	0.4	4.5	9.50
6	0.5	0.4	8.0	16.0
(b) variation of water partial pressure at fixed "medium" CO partial pressure of 3.8 bar				
7	4.3	3.8	1.0	0.23
8	4.3	3.8	4.5	1.05
9	3.4	3.0	8.0	2.33
(c) variation of water partial pressure at fixed "high" CO partial pressure of 6.7 bar				
10	7.7	6.7	1.0	0.13
11	7.7	6.7	4.5	0.58
12	7.7	6.7	8.0	1.04
(d) variation of CO/syngas partial pressure at fixed "low" water partial pressure of 1.0 bar				
4	0.5	0.4	1.0	2.10
7	4.3	3.8	1.0	0.23
10	7.7	6.7	1.0	0.13
(e) variation of CO/syngas partial pressure at fixed" medium"water partial pressure of 4.5 bar				
5	0.5	0.4	4.5	9.50
13	1.9	1.7	4.5	2.33
8	4.3	3.8	4.5	1.05
11	7.7	6.7	4.5	0.58
(f) variation of CO/syngas partial pressure at fixed "high" water partial pressure of 8.0 bar				
6	0.5	0.4	8.0	16.0
14	1.9	1.7	8.0	4.21
9	3.4	3.0	8.0	2.33
12	7.7	6.7	8.0	1.04

[a]Note that water partial pressures were realized via water co-feeding; syngas conversions were kept below 15%.

These analyses qualitatively confirm the trends as observed in the magnetic setup with crystallite sintering as a function of the reaction conditions (see Figure 7). Although at conditions of low water and low CO partial pressure, no sintering was obtained, and small crystallites (5−10 nm), mainly present in clusters, are observed. In addition, very severe sintering was found in samples exposed to conditions with high water and high CO partial pressures. Furthermore, at high CO/syngas partial pressures and medium to high water partial pressures,

DOI: 10.1021/cs501810y
ACS Catal. 2015, 5, 841−852

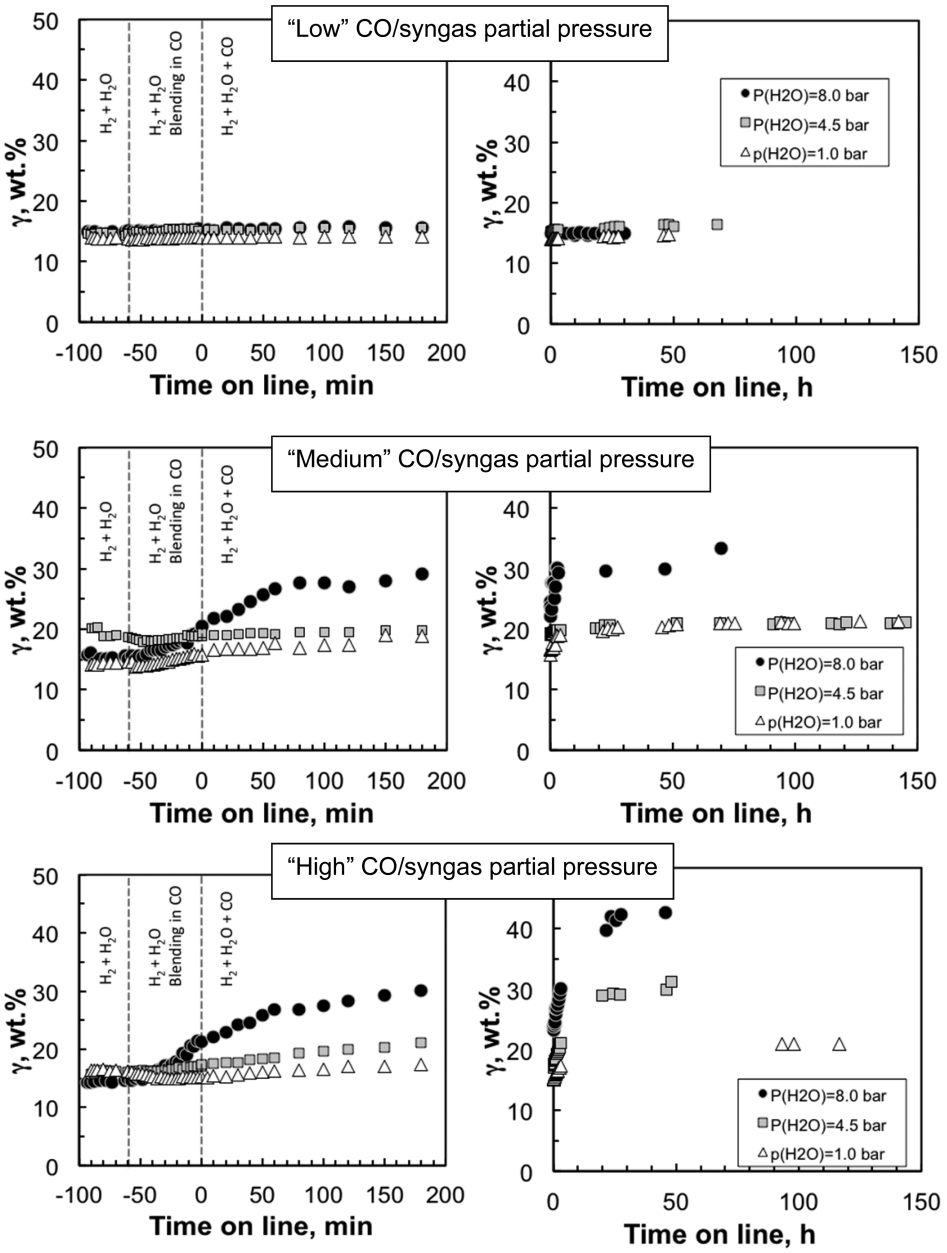

Figure 4. Weight percentage of cobalt displaying remnant magnetization, γ, during exposure to FTS conditions at fixed CO/syngas pressure levels (top: "low"; middle: "medium"; bottom: "high" CO/syngas pressure) and variation of water partial pressure.

the formation of carbon nanofibers was detected and confirmed by means of EDX analyses (see also Figure 8). This nanofiber formation seems to be catalyzed by large cobalt crystallites (up to 50 nm) detached from the support material, a phenomenon well-known from, for example, methane steam reforming using nickel catalysts (albeit at significantly higher temperatures).[7] In these catalysts, some cobalt is still present in small crystallites located in clusters.

At conditions of high water partial pressure, the trans-formation of the support to needle-like structures was observed (see Figure 7, e.g., run number 9). This is indicative of the formation of boehmite (AlOOH).[60] In combination with medium CO partial pressure, the formation of larger crystallites (up to 25 nm) was detected, but without formation of carbon nanotubes. At milder conditions, no severe sintering or formation of carbon fibers and/or boehmite formation are observed. Conditions of high CO and water partial pressures may however be problematic for supported cobalt FT catalysts, certainly for the alumina-supported catalyst used in this study.

The role of water versus the role of water in combination with CO/syngas on sintering was investigated in two additional experiments conducted at 230 °C in which the water to hydrogen ratio was varied over a very large range: in the first experiment no CO was present, whereas in the second one, a H_2/CO mixture was used (H_2/CO = 1.1). The reaction conditions are given in Figure 9. The experiments were started under hydrogen (8 bar). Water (2 bar) was introduced after 1 h while increasing the total reactor pressure correspondingly. The water partial pressure was then further increased every hour (with corresponding increase of total pressure) until 8 bar water was reached. From then on, the hydrogen partial pressure was reduced. In doing so, the water to hydrogen ratio was varied from 0 to 50. Subsequently, hydrogen was replaced with argon so that water was the only reactant still present. As

DOI: 10.1021/cs501810y
ACS Catal. 2015, 5, 841−852

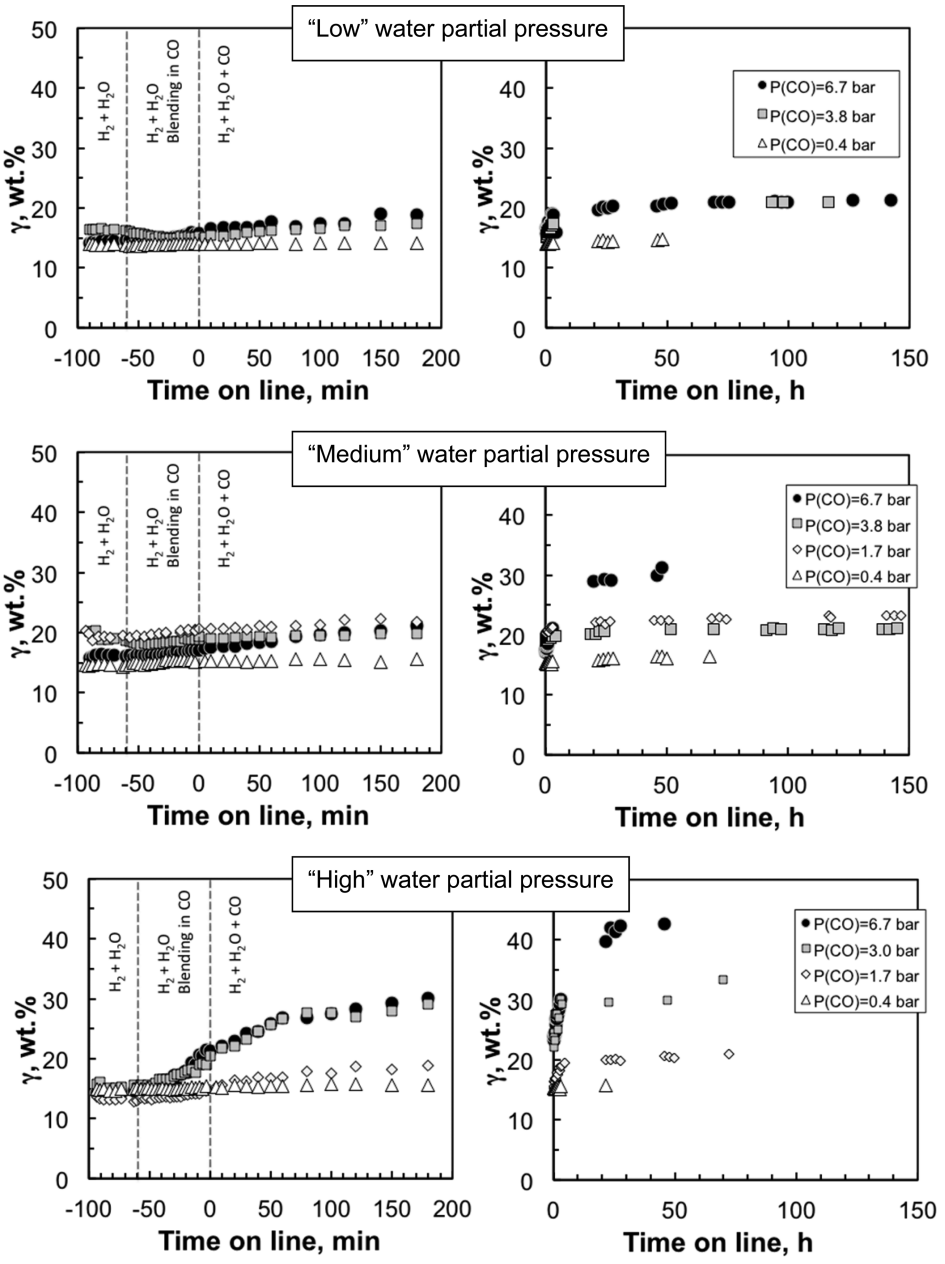

Figure 5. Weight percentage of cobalt displaying remnant magnetization, γ, during exposure to FTS conditions at water partial pressure levels (top: "low"; middle: "medium"; bottom: "high" water partial pressure) and variation of CO/syngas partial pressure.

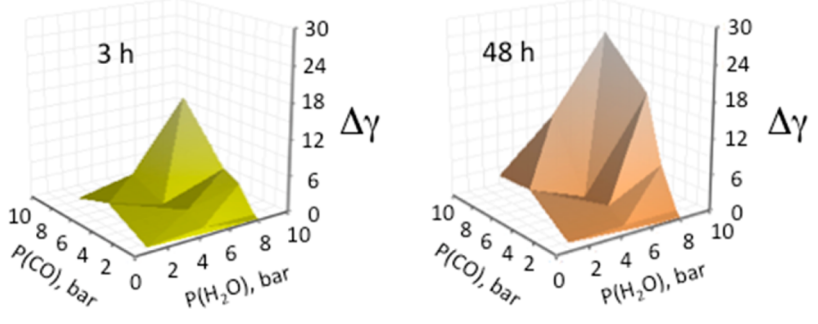

Figure 6. Change of weight percentage of cobalt displaying remnant magnetization, $\Delta\gamma$, as an indicator for sintering after 3 h (left) and after 48 h (right) during exposure to FTS conditions at different reaction conditions.

previously, the introduction of water (in both experiments) led to a slight increase of the saturation magnetization (Figure 9 left), due to electronic effect of adsorbed O and OH species. In the hydrogen–water atmosphere only a decrease of the

DOI: 10.1021/cs501810y
ACS Catal. 2015, 5, 841–852

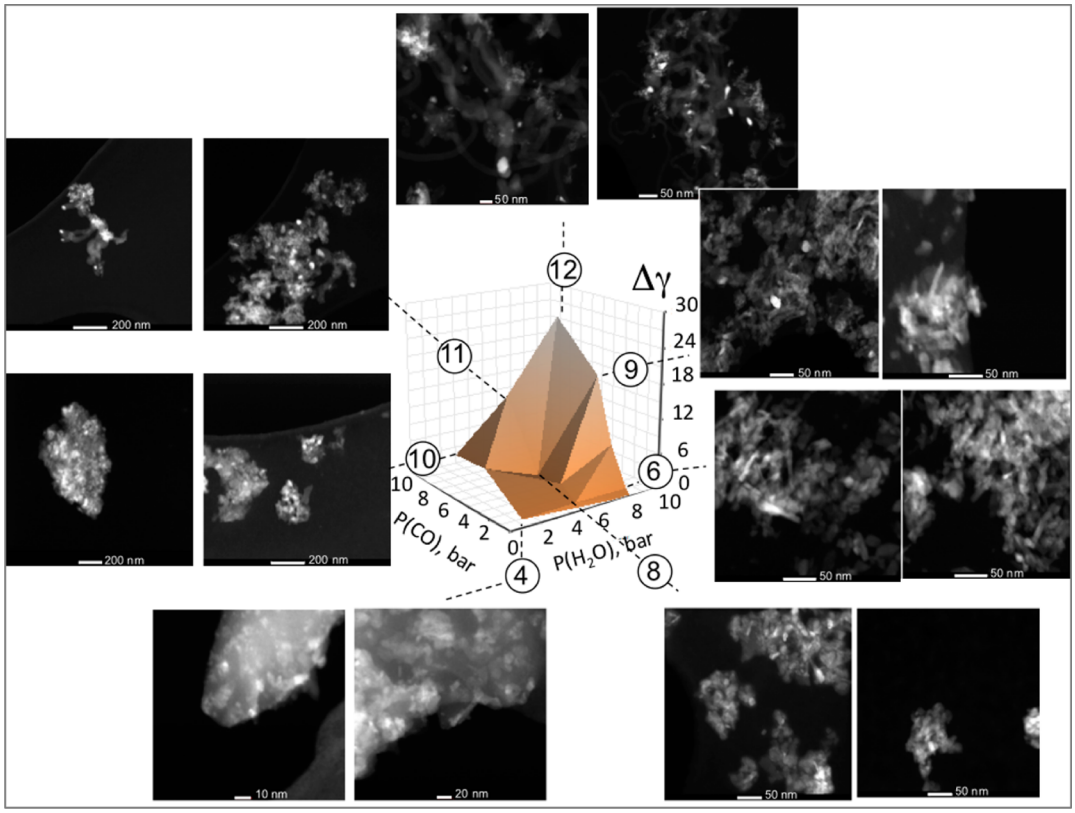

Figure 7. Overview of sintering behavior as a function of CO and water partial pressures. TEM analyses for selected spent catalyst samples (run numbers are encircled in the graph; for reaction conditions see Table 3).

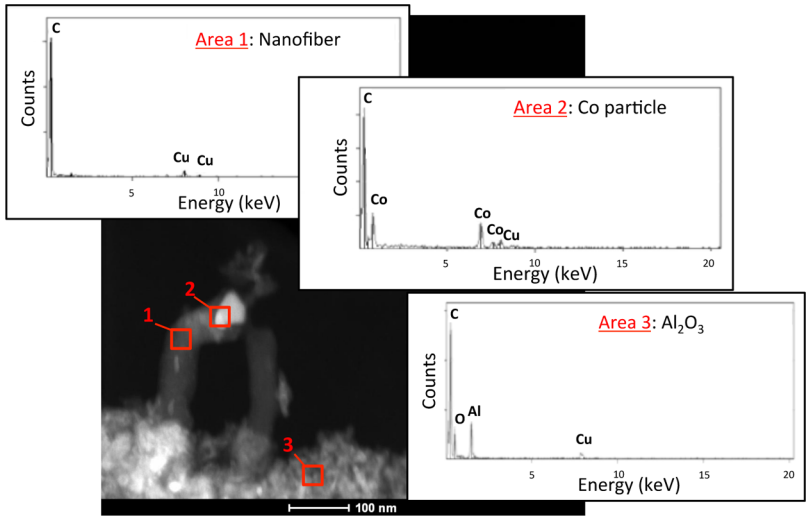

Figure 8. STEM-HAADF picture of spent catalyst (run 11: high CO and medium water partial pressures) and EDX analyses of three different areas (note that the copper signal is due to the grid which was used).

magnetization was observed at a water to hydrogen ratio of around 5:1 which may be due to the thermodynamically driven oxidation of small crystallites,[22] which recently could also be confirmed experimentally.[23] Only when hydrogen was removed from the feed did we observe a spontaneous oxidation of the catalyst, indicating the stabilizing role of hydrogen with regard to oxidation, which was earlier also observed by means of in situ Mössbauer analyses by Bezemer et al.[10] Interestingly, in the corresponding experiment in which syngas was used instead of hydrogen, no decrease in the saturation magnetization was observed until no more syngas was fed. This is probably due to the absence of very small crystallites at these conditions in this run, as sintering was observed in the presence of syngas, whereas virtually no sintering took place in the water hydrogen atmosphere only (see Figure 9 right). This experiment yet again shows very clearly that sintering occurs via a combination of water and CO.

4. DISCUSSION

The in situ setup for magnetic measurements allowed the following of sintering as a function of process parameters in real

DOI: 10.1021/cs501810y
ACS Catal. 2015, 5, 841−852

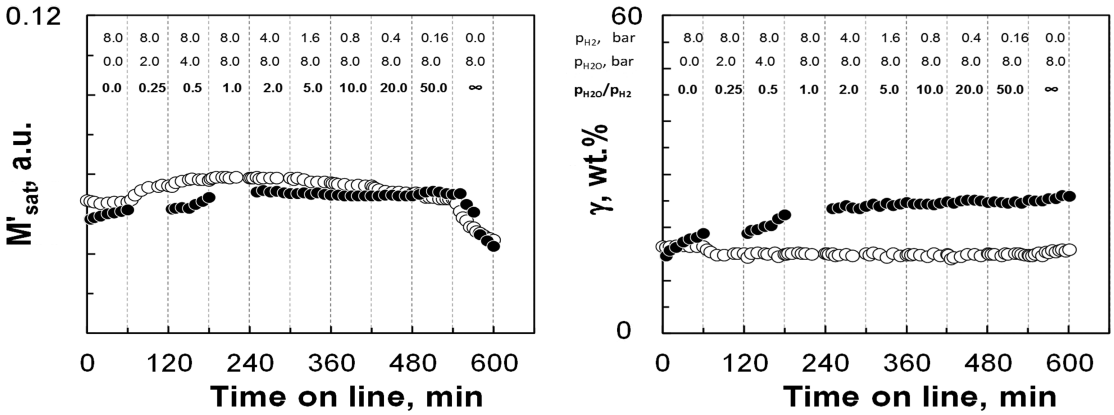

Figure 9. Saturation magnetization, per gram of cobalt in catalyst, (left) and weight percentage of cobalt displaying remnant magnetization, γ, (right) during exposure to different water to hydrogen ratios, with (●) and without CO (○).

time. It could be shown that severe conditions of high CO and high water partial pressure are highly conducive to severe sintering. In extreme cases of high CO or syngas pressure, respectively, and high water partial pressure, which may be important for process intensification, even the formation of carbon nanofibers under catalyst breakup can occur with the alumina-supported catalyst tested in this work.

Although in water−hydrogen mixtures, no sintering was observed with this catalyst at a reaction temperature of 230 °C, sintering was typically observed the moment CO was introduced with the feed stream (see Figures 2, 4, and 9). This seems to suggest a CO-assisted mechanism of sintering, possibly via Ostwald ripening involving cobalt (sub)carbonyl-type species as proposed for Rh on TiO_2.[61] However, more severe sintering was observed at increased temperatures (Figure 3), at which carbonyl formation is normally less favorable thermodynamically. Kinetic effects may therefore dominate. Alternatively, it may be speculated that the observed sintering effects might be due to temperature effects, that is, via heat locally generated by the FT reaction on the surface of the crystallite, as effects of severe sintering were typically observed where high FT rates can be expected. It may be noted that these local temperatures may not be measurable as the thermocouple, even though inserted directly into the catalyst bed, only detects temperature on a macroscopic scale (the temperature fluctuations during the experiments were within ±1 °C). However, the experiment where the catalyst was tested in the hydrogen/water atmosphere (Figure 3) suggests that only extremely high temperatures of approximately 350 °C can account for severe sintering effects in the absence of CO.

It is therefore hypothesized that sintering can be CO assisted and that it is accelerated in the presence of water. Indeed, at low water levels, almost no sintering could be detected. Water may be impacting on the catalyst surface, possibly even modifying/changing it, and in particular the surface of the support. TEM characterization of the catalyst exposed to conditions of high water partial pressure saw the formation of needle-like structures (typically associated with AlOOH), supporting the notion that the alumina carrier undergoes changes in the presence of product water. This may include formation of hydroxyl groups and weakening of local metal−support interaction. It may further be speculated that the clustered arrangement of the cobalt nanoparticles in the catalyst may facilitate sintering due to the vicinity of the cobalt crystallites in the clusters. Sintering on the time-scale observed previously may be restricted to cobalt within these clusters.[29] The combined effect of water and carbon monoxide on the rate of sintering suggests that the transport of these cobalt carbonyl species does not occur via the gas phase but rather via transport over a water-modified alumina support surface (see Figure 10).

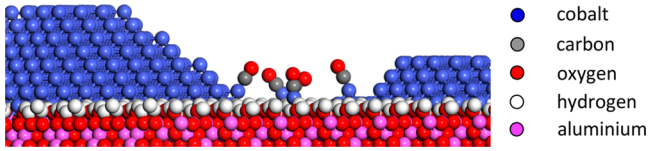

Figure 10. Proposed scheme of sintering via cobalt subcarbonyl species transport over hydroxylated alumina surface.

Previously, researchers at Shell proposed that cobalt subcarbonyls, $Co(CO)_x$ (x = 1−3), are responsible for the movement of Co atoms at moderate pressures (4 bar) resulting in restructuring of cobalt surfaces.[62] Formation of these subcarbonyls may lower the activation energy for metal atom migration, and sintering can occur at low temperatures and pressure (a process known for nickel FTS catalysts[63]). As opposed to full carbonyls, where transport is in the gas phase, these metal subcarbonyls are mobile over the support. It should be noted that the proposed mechanism via Ostwald ripening and the involvement of CO plus water is in contrast to the particle migration/coalescence mechanism proposed for sintering in the cobalt-based Fischer−Tropsch synthesis by others (Kiss et al.,[11,12] Khodakov et al.,[15,20,21] Tsoukamis et al.,[32] Bezemer et al.[10]). It should however be noted that particle coalescence should generally be less likely at the low temperature conditions of the cobalt FTS.

Assuming that the above-proposed mechanism is correct, an improvement of cobalt-based catalysts with regard to sintering may be achieved by a better distribution of cobalt particles over the support in order to avoid cluster formation and to circumvent the use of supports that allow for mobility of cobalt subcarbonyl species. Alternatively, for a given catalyst reaction, conditions must be chosen such that severe sintering does not play a dominant role. Lastly, the observations made here may be limited to supports that allow the formation of hydroxyl groups, which enable subcarbonyl mobility. The in situ setup for magnetic measurements is an ideal and unique tool to determine the thresholds at which sintering occurs.

DOI: 10.1021/cs501810y
ACS Catal. 2015, 5, 841−852

5. CONCLUSIONS

Sintering as a function of process condition was followed in real time using the in situ setup for magnetic measurements. The alumina-supported cobalt catalyst did not show any sintering in water−hydrogen atmospheres at typical FT reaction temperatures. Significant changes of crystallite size could only be observed in the presence of water and CO. It is hypothesized that sintering is CO assisted, possibly via a surface subcarbonyl-type mechanism, on the water-modified alumina support surface.

AUTHOR INFORMATION

Corresponding Author

*E-mail: Michael.Claeys@uct.ac.za.

Notes

The authors declare no competing financial interest.

ACKNOWLEDGMENTS

Assistance regarding TEM measurements by Dr. Theresa Feltes is greatly acknowledged. Dr. Jan-Albert van den Berg, Dr. Melissa Petersen, and Dr. Ionel Ciobîcă are acknowledged for their assistance in providing the computational data.

REFERENCES

(1) van de Loosdrecht, J.; Botes, F. G.; Ciobîca, I. M.; Ferreira, A.; Gibson, P.; Moodley, D. J.; Saib, A. M.; Visagie, J. L.; Weststrate, C. J.; Niemantsverdriet, J. W. Fischer−Tropsch Synthesis: Catalysts and Chemistry. In *Comprehensive Inorganic Chemistry II*; Reedijk, J., Poeppelmeier, K., Eds.; Elsevier: Oxford, 2013; Vol 7, pp 525−557.

(2) Tsoukamis, N. E.; Rønning, M.; Borg, Ø.; Rytter, E.; Holmen, A. *Catal. Today* **2010**, *154*, 162−182.

(3) Bartholomew, C. H. *Appl. Catal., A* **2001**, *212*, 17−60.

(4) Overett, M. J.; Breedt, B.; Du Plessis, E.; Erasmus, W.; van de Loosdrecht, J. *Prepr. Pap.-Am. Chem. Soc., Div. Petr. Chem.* **2008**, *53*, 126−128.

(5) Saib, A. M.; Moodley, D. J.; Ciobîca, I. M.; Hauman, M. M.; Sigwebela, B. H.; Westrate, C. J.; Niemantsverdriet, C. W.; van de Loosdrecht, J. *Catal. Today* **2010**, *154*, 271−282.

(6) Moulijn, J. A.; van Diepen, A. E.; Kapteijn, F. *Appl. Catal., A* **2001**, *212*, 3−16.

(7) Sehested, J.; Gelten, J. E. P.; Helveg, S. *Appl. Catal., A* **2006**, *309*, 237−246.

(8) Parker, S. C.; Campbell, C. T. *Phys. Rev. B* **2007**, *75*, 035430.

(9) Bian, G.-Z.; Fujishita, N.; Mochizuki, T.; Ning, W.-S.; Yamada, M. *Appl. Catal., A* **2003**, *252*, 251−260.

(10) Bezemer, G. L.; Remans, T. J.; van Bavel, A. P.; Dugulan, A. I. *J. Am. Chem. Soc.* **2010**, *132*, 8540−8541.

(11) Kiss, G.; Kliewer, C. E.; DeMartin, G. J.; Culross, C. C.; Baumgartner, J. E. *J. Catal.* **2003**, *217*, 127−140.

(12) Kliewer, C. E.; Kiss, G.; Soled, S. L. *Microsc. Microanal.* **2010**, *16* (Suppl 2), 12581259.

(13) Karaca, H.; Hong, J.; Fongarland, P.; Roussel, P.; Griboval-Constant, A.; Lacroix, M.; Hortman, K.; Safonova, O. V.; Khodakov, A. Y. *Chem. Commun.* **2010**, *46*, 788−790.

(14) Karaca, H.; Safonova, O. V.; Chambrey, S.; Fongarland, P.; Roussel, P.; Griboval-Constant, A.; Lacroix, M.; Khodakov, A. Y. *J. Catal.* **2011**, *277*, 14−26.

(15) Sadeqzadeh, M.; Chambrey, S.; Hong, J.; Fongarland, P.; Luck, F.; Curulla-Ferré, D.; Schweich, D.; Bousquet, J.; Khodakov, A. Y. *Ind. Eng. Chem. Res.* **2014**, *53*, 6913−6922.

(16) Zhou, W.; Chen, J.-G.; Fang, K. G.; Sun, Y.-H. *Fuel Process. Technol.* **2006**, *87*, 609−616.

(17) Sehested, J. *J. Catal.* **2003**, *217*, 417−426.

(18) Sehested, J.; Gelten, J. A. P.; Remediakis, I. N.; Bengaard, H.; Nørkov, J. K. *J. Catal.* **2004**, *223*, 432−443.

(19) Sehested, J.; Larsen, N. W.; Falsi, H.; Hinnemann, B. *Catal. Today* **2014**, *228*, 22−31.

(20) Sadeqzadeh, M.; Hong, J.; Fongarland, P.; Curulla-Ferré, D.; Luck, F.; Bousquet, J.; Schweich, D.; Khodakov, A. Y. *Ind. Eng. Chem. Res.* **2012**, *51*, 11955−11964.

(21) Sadeqzadeh, M.; Chambrey, S.; Piché, S.; Fongarland, P.; Luck, F.; Curulla-Ferré, D.; Schweich, D.; Bousquet, J.; Khodakov, A. Y. *Catal. Today* **2013**, *215*, 52−59.

(22) van Steen, E.; Claeys, M.; Dry, M. E.; van de Loosdrecht, J.; Viljoen, E. L.; Visagie, J. L. *J. Phys. Chem. B* **2005**, *109*, 3575−3577.

(23) Fischer, N.; Clapham, B.; Feltes, T.; van Steen, E.; Claeys, M. *Angew. Chem., Int. Ed.* **2014**, *53*, 1342−1345.

(24) Jacobs, G.; Zhang, Y.; Das, T. K.; Li, J.; Patterson, P. M.; Davis, B. H. *Stud. Surf. Sci. Catal.* **2001**, *139*, 415−422.

(25) Jacobs, G.; Patterson, P. M.; Zhang, Y.; Das, T.; Li, J.; Davis, B. H. *Appl. Catal., A* **2002**, *233*, 215−226.

(26) Das, T. K.; Jacobs, G.; Patterson, P. M.; Conner, W. A.; Li, J.; Davis, B. H. *Fuel* **2003**, *82*, 805−815.

(27) Jacobs, G.; Sarkar, A.; Ji, Y.; Luo, M.; Dozier, A.; Davis, B. H. *Ind. Eng. Chem. Res.* **2008**, *47*, 672−680.

(28) Jacobs, G.; Ma, W.; Gao, P.; Todic, B.; Bhatelia, T.; Bukur, D.; Davis, B. H. *Catal. Today* **2013**, *214*, 100−139.

(29) van de Loosdrecht, J.; Balzhinimaev, B.; Dalmon, J. A.; Niemantsverdriet, J. W.; Tsybulya, S. V.; Saib, A. M.; van Berge, P. J.; Visagie, J. L. *Catal. Today* **2007**, *123*, 293−302.

(30) Rønning, M.; Tsakoumis, N. E.; Voronov, A.; Johnsen, R. E.; Norby, P.; van Beek, W.; Borg, Ø.; Rytter, E.; Holmen, A. *Catal. Today* **2010**, *155*, 289−295.

(31) Tsakoumis, N. E.; Dehghan, R.; Johnsen, R. E.; Voronov, A.; van Beek, W.; Walmsley, J. C.; Borg, Ø.; Rytter, E.; Chen, D.; Rønning, M.; Holmen, A. *Catal. Today* **2013**, *205*, 86−93.

(32) Tsakoumis, N. E.; Dehghan-Niri, R.; Rønning, M.; Walmsley, J. C.; Borg, Ø.; Rytter, E.; Holmen, A. *Appl. Catal., A* **2014**, *479*, 59−69.

(33) Tavasoli, A.; Irani, M.; Abbaslou, R. M. M.; Trépanier, M.; Dalai, A. K. *Can. J. Chem. Eng.* **2008**, *86*, 1070−1080.

(34) Tavasoli, A.; Abbaslou, R. M. M.; Dalai, A. K. *Appl. Catal., A* **2008**, *346*, 58−64.

(35) Datye, A. K.; Xu, Q.; Kharas, K. C.; McCarty, J. M. *Catal. Today* **2006**, *111*, 59−67.

(36) Hauman, M. M.; Saib, A. M.; Moodley, D. J.; du Plessis, E.; Claeys, M.; van Steen, E. *ChemCatChem.* **2012**, *4*, 1411−1419.

(37) Thüne, P. C.; Westrate, C. J.; Moodley, P.; Saib, A. M.; van de Loosdrecht, J.; Miller, J. T.; Niemantsverdriet, J. W. *Catal. Sci. Technol.* **2011**, *1*, 689−697.

(38) Claeys, M.; van Steen, E.; Visagie, J. L.; van de Loosdrecht, J. A Magnetometer for in-situ Characterisation of Ferromagnetic Materials and Catalysts. South African Patent 2010/08984, Aug 31, 2011.

(39) Claeys, M.; van Steen, E.; du Plessis, E.; Van Berge, P. J.; Saib, A. M.; Moodley, D. J. *J. Catal.* **2014**, *318*, 193−202.

(40) van Berge, P. J.; van de Loosdrecht, J.; Visagie, J. L. (Sasol Technology Pty Ltd, RSA) Cobalt Catalysts, United States Patent US 6,806,226, October 19, 2004.

(41) Selwood, P. W. *Chemisorption and Magnetism*; Academic Press: New York, San Francisco, London, 1975.

(42) Billas, I. M. L.; Chatelain, A.; De Heer, W. A. *Science* **1994**, *265*, 1682−1684.

(43) Dalmon, J. A. Magnetic Measurements and Catalysis. In *Catalyst Characterisation: Physical Techniques for Solid Materials*; Imelik, B., Vedrine, J. C., Eds.; Plenum Press: New York, 1994; pp 585−641.

(44) Barbier, A.; Hanif, A.; Dalmon, J. A.; Martin, G. A. *Appl. Catal., A* **1998**, *168*, 333−343.

(45) Barbier, A.; Martin, G. A.; Ramirez de la Piscina, P.; Homs, N. *Appl. Catal., A* **2001**, *210*, 75−81.

(46) Bean, C. P.; Livingston, J. D. *J. Appl. Phys.* **1959**, *30*, 120−129.

(47) Kresse, G.; Hafner, J. *Phys. Rev. B* **1993**, *47*, 558−561.

(48) Kresse, G.; Furthmüller, J. *Phys. Rev. B* **1996**, *54*, 11169−11186.

(49) Perdew, J. P.; Wang, Y. *Phys. Rev.* **1992**, *45*, 13244−13249.

(50) Methfessel, M.; Paxton, A. T. *Phys. Rev. B* **1989**, *40*, 3616−3621.

(51) Monkhorst, H. J.; Pack, J. D. *Phys. Rev. B* **1976**, *13*, 5188−5192.

DOI: 10.1021/cs501810y
ACS Catal. 2015, 5, 841−852

(52) Murnaghan, F. D. *Proc. Natl. Acad. Sci. U.S.A.* **1944**, 244−247.
(53) Birch, F. *Phys. Rev.* **1947**, *71*, 809−824.
(54) Ashcroft, N. W.; Mermin, N. D. *Solid State Physics*; Holt, Rinehart and Winston: New York, 1976.
(55) Mehl, M. J.; Papaconstantopoulos, D. A. *Phys. Rev. B* **1996**, *54*, 4519−4530.
(56) West, A. R. *Basic Solid State Chemistry*, 2nd ed.; John Wiley & Sons Ltd.: New York, 1999.
(57) Mattson, R.; Mattson, A. E. *Phys. Rev. B* **2002**, *66*, 214110−214117 http://dft.sandia.gov/functionals/webcalculator.html,.
(58) Lide, D.; Kehiaian, H. *CRC Handbook of Thermophysical and Thermochemical Data*; CRC Press: Boca Raton, FL, 1994.
(59) van Helden, P.; Ciobîcă, I. M. *ChemPhysChem* **2011**, *12*, 2925−2928.
(60) De Souza Santos, P.; Vieira Coehlo, A. C.; de Souza Santos, H.; Kunihiko Kiyohara, P. *Mater. Res.* **2009**, *12* (4), 437−445.
(61) Ouyang, R.; Liu, J.-X.; Li, W.-X. *J. Am. Chem. Soc.* **2013**, *135*, 1760−1771.
(62) Wilson, J.; De Groot, C. *J. Phys. Chem.* **1995**, *99*, 7860−7866.
(63) Agnelli, M.; Kolb, M.; Miradatos, C. *J. Catal.* **1994**, *148*, 9−21.

DOI: 10.1021/cs501810y
ACS Catal. 2015, 5, 841−852